Eur. Phys. J. D (2017) 71: 302
DOI: 10.1140/epjd/e2017-80259-6

THE EUROPEAN PHYSICAL JOURNAL D

Regular Article

A parametric study of the microwave plasma-assisted combustion of premixed ethylene/air mixtures

Che A. Fuh, Wei Wu, and Chuji Wang[a]

Department of Physics and Astronomy, Mississippi State University, Starkville, MS 39759, USA

Received 17 April 2017 / Received in final form 6 September 2017
Published online 23 November 2017 – © EDP Sciences, Società Italiana di Fisica, Springer-Verlag 2017

Abstract. A parametric study of microwave argon plasma assisted combustion (PAC) of premixed ethylene/air mixtures was carried out using visual imaging, optical emission spectroscopy and cavity ringdown spectroscopy as diagnostic tools. The parameters investigated included the plasma feed gas flow rate, the plasma power, the fuel equivalence ratio and the total flow rate of the fuel/air mixture. The combustion enhancement effects were characterized by the minimum ignition power, the flame length and the fuel efficiency of the combustor. It was found that: (1) increasing the plasma feed gas flow rate resulted in a decrease in the flame length, an increase in the minimum ignition power for near stoichiometric fuel equivalence ratios and a corresponding decrease in the minimum ignition power for ultra-lean and rich fuel equivalence ratios; (2) at a constant plasma power, increasing the total flow rate of the ethylene/air mixture from 1.0 slm to 1.5 slm resulted in an increase in the flame length and a reduction in the fuel efficiency; (3) increasing the plasma power resulted in a slight increase in flame length as well as improved fuel efficiency with fewer C_2(d) and CH(A) radicals present downstream of the flame; (4) increasing the fuel equivalence ratio caused an increase in flame length but at a reduced fuel efficiency when plasma power was kept constant; and (5) the ground state OH(X) number density was on the order of 10^{15} molecules/cm^3 and was observed to drop downstream along the propagation axis of the flame at all parameters investigated. Results suggest that each of the parameters independently influences the PAC processes.

1 Introduction

Plasma assisted combustion is a relatively new research thrust by the scientific community in the recent decades urged on by the need to solve the drawbacks of traditional non plasma assisted combustion (PAC) such as the inability to operate in adverse flow conditions, long ignition delay times, low flammability limits, etc. Researchers have been able to show that the addition of a plasma to a conventional fuel/oxidant mixture results in reduced minimum ignition limit [1–3], improved flame stabilization and flame holding [4–7], reduced ignition delay time [8–10], etc. For example, researchers such as Varella et al. [11] used a plasma generated by a gliding arc discharge to investigate the effects of plasma on pollutant emission in the PAC of natural gas at rich fuel equivalence ratios. They observed a reduction in hydrocarbons and carbon monoxide in the exhaust gases with the use of plasmas indicating improved fuel efficiency. Yamamoto et al. [12] investigated the characteristics of combustion and reformation of plasma-assisted combustion in spray combustion using a non-equilibrium microwave plasma. They observed an increase in radicals generated by the plasma and combustion temperature with increase in the plasma power. They also observed a decrease in the unburnt fuel percentage in the combustor exhaust and reported the cold gas efficiencies under microwave input powers of 350 W and 750 W in the case of PAC to be 1.6 and 2.1 times higher than in the case of normal combustion. Hwang et al. [13] carried out an experimental study to investigate the effect of a microwave-assisted plasma ignition in acetylene/air mixtures over various fuel equivalence ratios and initial ambient pressures. They observed an extension in the lean burn limit with microwave plasma assisted ignition compared to conventional spark ignition and also recorded a decrease in flame development time with a 20% increase in flame speed. Bao et al. [14] also investigated the ability of a high voltage nanosecond pulse duration, high repetition rate plasma to generate radicals. The radicals generated, caused an increase in temperature resulting in flow ignition and improved flameholding in methane/air and ethylene/air mixtures. Previously, we have demonstrated the ability of a microwave plasma to reduce the lean burn limit, assist in ignition under extreme conditions, improve on stabilization and flameholding in the plasma assisted ignition and combustion of methane and ethylene with different oxidants [2,4,17,18], etc. Other recent works studying the enhancement effects of the addition of plasmas to the combustion process are found in the reviews [19–21].

Even though the addition of a plasma to the combustion process has been shown to have all the above stated enhancement effects such as reduced ignition delay

[a] e-mail: cw175@msstate.edu

time, improved flame holding, etc., the exact mechanism through which the plasma brings about the observed enhancement effects is still not very clear. This is due to the many different sources of plasmas with different compositions as well as various fuel/oxidants combinations employed in PAC applications. Hence, in this study we employed a 2.45 GHz microwave plasma source to generate an argon microwave plasma which we used to conduct a parametric investigation on the plasma assisted ignition and combustion of a premixed ethylene/air mixture. This was in a bid to better understand the mechanisms through which the plasma enhanced the combustion process since it is important to know how each individual plasma or fuel/oxidant parameter independently influences the plasma assisted ignition and combustion process. The plasma and fuel/air mixture parameters investigated were the plasma power, the plasma feed gas flow rate, the fuel equivalence ratio of the fuel/air mixture and the total flow rate of the premixed fuel/air mixtures introduced into the system. The criteria employed to judge the enhancement effects of the plasma on the ignition and combustion process were the minimum ignition power, the flame length and the fuel efficiency of the combustion process. Initially, the argon plasma feed gas flow rate was varied to investigate the effect of the size of the radical pool generated by the plasma on combustion enhancement. Secondly, the plasma power was varied to investigate the effect of the thermal contribution of the plasma on the combustion process. The total flow rate and fuel equivalence ratios were also varied to shed more light on the effect of fuel/air mixture composition and flow rate on the enhancements observed in the PAC process. The experimental setup used in this study is presented in Section 2 with the results and conclusion presented in Sections 3 and 4 respectively.

2 Experimental setup

Figure 1 shows the schematic of the experimental system which consisted of three major sections: a microwave plasma-assisted combustion reactor, a gas flow control manifold, and a suite of optical diagnostic systems made up of a digital imaging system, a fiber-guided optical emission spectroscopy (OES) system, and a pulsed cavity ringdown spectroscopy (CRDS) system. Each of these sections is briefly described below.

2.1 Microwave plasma-assisted combustion reactor

Figure 2 illustrates the configuration of the microwave plasma-assisted combustion reactor. The reactor was composed of an in-house built microwave plasma cavity and a T-shaped quartz tube (combustor) with inner and outer diameters of 2 mm and 6 mm, respectively. The microwave plasma cavity was made of a cylindrically shaped copper tube with a cross-sectional diameter of 5 cm and a cavity length of 8 cm. This type of microwave plasma cavity is often referred to as a microwave plasma surfatron. A 2.45 GHz microwave plasma source (AJA International) was connected to the cavity by a 0.6 m long low-loss coaxial cable (LMR-400, Times Microwave Systems) with an attenuation rate of $0.144\,\mathrm{dBm}^{-1}$ at 2.45 GHz (equivalent to a 2% transmission loss in the cable). The plasma power was transmitted in the TEM_{00} mode, and the cavity excitation coupling was optimized for a reflective power of 2–8 W with a forward power of 60–160 W. The 2% transmission loss in the cable added to the 3–5% reflected power losses resulted in a total power loss of between 5% and 7%. No exact power loss in the coupling process of the plasma to the fuel/air mixture was measured for all powers investigated. Given the low percentage power loss and constancy of this loss for all forward powers investigated, it is inferred that, the overall trends observed by varying the plasma power in this parametric study are not affected. As a result, emphasis in this study is placed on the trends observed with power variation and not on individual power measurements alone. Hence throughout the paper, the plasma power refers to the forward power from the microwave plasma generator. As shown in Figure 2, the horizontal arm of the T-shaped quartz tube was inserted through the cylindrical axis (x-axis) of the microwave cavity. Argon plasma feed gas flowed through this arm and formed a continuous plasma jet propagating along the arm from the microwave cavity orifice to the joint part of the T-shaped combustor. The vertical arm of the T-shaped quartz tube was used to inject ethylene/air mixtures from the lower end. The ethylene/air mixtures was coupled to the argon plasma jet perpendicularly at the joint part of the combustor, and then propagated out from the upper end of the vertical arm in the form of plasma-assisted combustion flame. Due to the efficient plasma generation in the surfatron, no cooling device was needed when the plasma-assisted combustion reactor was operated continuously for more than 10–12 h.

2.2 Gas flow control manifold

The gas manifold consists of three flow meters: the first flow meter was used to adjust ethylene gas flow rate in the range of 0–396 standard cubic centimeter per minute (sccm); the second one was used for regulating the air flow rate regulation from 0 to 2.0 standard liter per minute (slm, 1 slm = 1000 sccm); and the last one was used to regulate the argon gas flow rate in the range of 0–1.78 slm. For a fixed total flow rate of the ethylene/air mixture, variation of the fuel equivalence ratio ϕ was achieved by adjusting the relative ratio of ethylene/air. The purities of argon gas and ethylene gas were 99.999% (Airgas) and 99.99% (Airgas). Ultra zero grade air obtained from Airgas was used in this study.

2.3 Digital imaging

This was used to capture plasma and flame structures. Images of the plasma plume and combustion flame were obtained using a digital camera (Sony, FCB-EX78BB) with a time resolution of 100 μs–1 s. The shutter speed was adjusted to optimize the visual effect of the plasma plume and combustion flame images. Since the plasma was continuous, no temporal behavior of the plasma-assisted

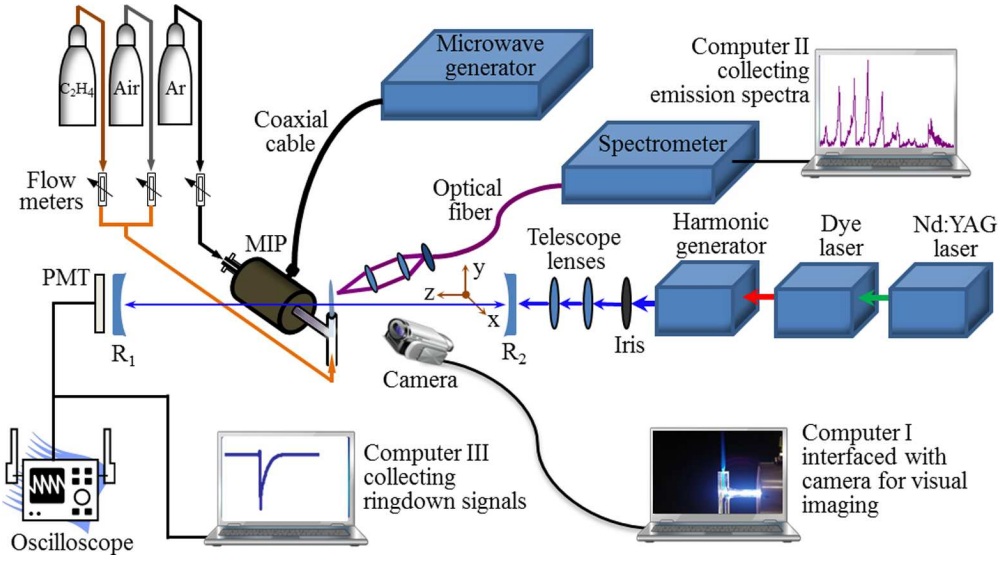

Fig. 1. Schematic of the experimental system that consists of the microwave plasma-assisted combustion reactor, the gas flow control manifold, and the optical diagnostic systems.

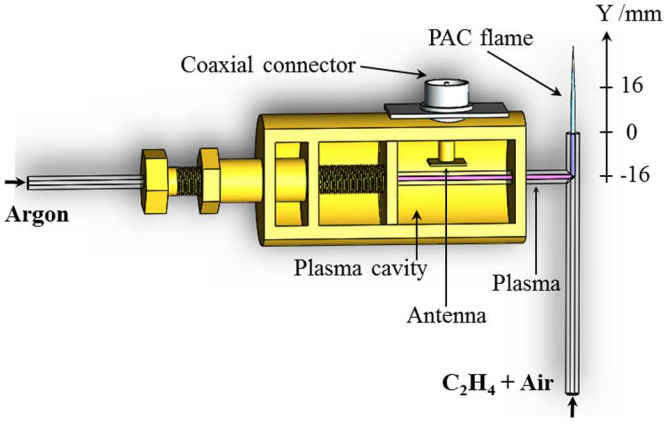

Fig. 2. Configuration illustration of the microwave plasma-assisted combustion reactor.

combustion was explored. The operation of the imaging system was controlled by Computer I.

2.4 Optical emission spectroscopy (OES) system

The OES system was applied to characterize the plasma and flame emissions at different locations of the combustor. Plasma and combustion flame emissions were collected perpendicularly to the combustor plane using two identical focal lenses ($f = 5.0$ cm), and the emissions were transmitted to a spectrometer (Avantes) via a section of optical fiber. The dual-channel spectrometer housed two gratings of 600 grooves mm^{-1} and 1200 grooves mm^{-1} separately to cover a spectral range of 200–660 nm with a resolution of 0.07 nm at 350 nm. The combustor was mounted on a high precision stage with a precision of $\pm 100\,\mu$m. Emissions spectra in the spectral range of 200–660 nm were obtained from the plasma and PAC flame at different locations. The integration time was adjusted according to emission intensities, ranging from 5 to 100 s. The OES system was operated by Computer II as shown in Figure 1.

2.5 CRDS system

The CRDS was employed to measure the absolute number densities of the electronic ground state species, e.g. OH(X). The ringdown cavity was constructed using a pair of high reflective ($R = 99.9\%$ at 308 nm) plano-concave mirrors of 6-m radius of curvature with a separation of 73 cm. The PAC flame was placed in the center of the ringdown cavity. The PAC flame was perpendicular to the optical axis (z-axis) of the ringdown cavity such that the laser beam passed through the cross-section of the PAC flame. By moving the combustor on a translation stage while keeping the laser beam fixed in space, the laser beam location in the flame was scanned with a spatial resolution of 2 mm along the y-axis. The laser beam pathlengths inside the PAC flame were estimated from the geometries of the PAC flame images. The UV laser beam was obtained from the frequency doubling (Inrad Autotracker III) of the output of a tunable narrow linewidth, dual grating dye laser (NarrowScan, Radiant), which was pumped by a 20 Hz Nd:YAG laser (Powerlite 8020, Continuum). The single pulse energy at 308 nm was a few μJ and the cross-section of the laser beam in the flame was 0.5 ± 0.1 mm^2. The minimum scanning step for the dye laser was 0.0005 nm. The ringdown signal was detected using a photomultiplier tube (PMT, R928, Hamamatsu) mounted with a 10 nm band pass interference filter to block the PAC emissions. Ringdown signals were monitored by an oscilloscope (TDS 410A, Tektronix) connected to Computer III running a home-developed ringdown software. A detailed description of the CRDS system can be

seen elsewhere [22,23]. The ringdown baseline noise averaged over 100 ringdown events was typically 0.5% and 0.8% without and with the PAC running, respectively.

3 Results and discussion

3.1 Plasma effect on minimum ignition power

Figure 3 shows the plot of the minimum power at which a flame was observed outside the combustor against the fuel equivalence ratio for three different argon plasma feed gas flow rates. This plot was obtained by increasing the plasma power from the minimum plasma power of 5 W at which the reactor can sustain a plasma, to the plasma power at which a flame was observed outside the combustor. The minimum ignition power investigations for all argon plasma feed gas flow rates were performed at a constant fuel/air mixture flow rate of 1.5 slm. It should be noted that for all argon flow rates investigated, the same U-shaped minimum ignition power curve as reported in reference [24] is obtained. The decrease in minimum ignition plasma power with increase in fuel equivalence ratio for lean fuel equivalence ratios is attributed to an increase in thermal energy released during the breakdown of the fuel with increase in fuel equivalence ratio upon establishment of the radical pool required for ignition. This higher thermal input from the breakdown process offsets the heat loss to the environment and thus requires a lower plasma power to initiate ignition. Hence for lower fuel equivalence ratios ($\phi = 0.4$–0.8), minimum ignition power is more dependent on thermal energy input from the plasma. For stoichiometric to rich fuel equivalence ratios ($\phi = 0.9$–1.4), the minimum plasma power required to ignite plasma increases with increase in fuel equivalence ratio. This observed trend is due to plasma quenching in the case of the higher fuel equivalence ratios due to the higher fuel concentration. Plasma quenching results in the generation of a smaller radical pool required for ignition thus requiring an increase in plasma power to generate the radical pool required for fuel breakdown and ignition to occur. Since plasma quenching increases with increase in the fuel equivalence ratio, a higher plasma power is therefore also required to ensure the generation of the required radical pool for ignition to occur, hence the observed trend. Thus, as observed, for lean fuel equivalence ratios, ignition is more dependent on plasma thermal input since plasma quenching is less apparent whereas for richer fuel equivalence ratios, ignition is more dependent on radical supplied by plasma due to a higher plasma quenching effect.

The variation in the minimum ignition power and the plasma feed gas flow rate can be explained by considering the flow dynamics in the surfatron. Srivastava and Wang [24] characterizing an atmospheric pressure helium microwave plasma jet observed that upon increasing the helium plasma feed gas at constant power, the OH(X) radical concentration at a fixed position increased to a peak concentration with increase in helium flow rate before dropping off. It is inferred from this study that increasing the plasma feed gas results in a larger radical pool supplied by the plasma since there is more gas available

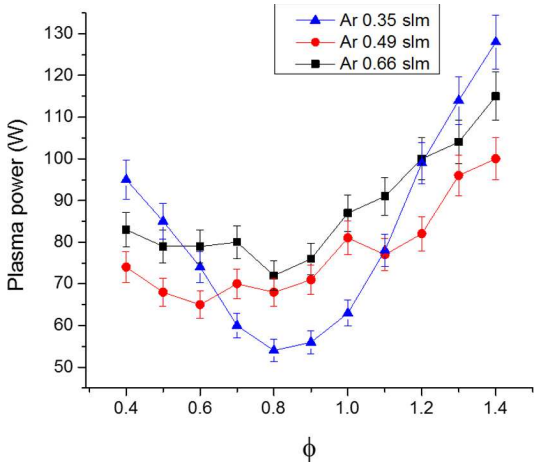

Fig. 3. Plot of minimum ignition plasma power (±7% uncertainty) at which a flame is observed outside the combustor vs fuel equivalence ratio (f) for argon plasma feed gas flow rates of 0.35 slm, 0.49 slm and 0.66 slm. The total flow rate was kept constant at 1.5 slm.

for ionization and radical generation along with a corresponding increase in turbulence in the plasma reactor. Hence, increasing plasma feed gas flow rate results in a larger radical pool generated which enhances ignition and flame stability while also increasing the turbulence generated in the combustor due to the larger gas flow. Evidence to further support the increase in radical pool and turbulence with increase in plasma feed gas flow rate is provided by the images below. An increase in plasma flow turbulence with a corresponding increase in plasma feed gas flow rate was also reported in references [25,26] where it was observed that increasing the plasma flow rate caused a transition from laminar to turbulent flow resulting in a decrease in the plasma jet length and stability. It is thus inferred from these studies that increasing the plasma feed gas flow rate results in a corresponding increase in turbulence in the combustor when the plasma is coupled to the fuel/air mixture. The evidence supporting the existence of the flow rates used in this study to be in the transition from the laminar to turbulent regime is obtained from the corresponding decrease in the flame length with increase in argon plasma flow rates as shown in Section 3.2. It was seen that for fuel equivalence ratios in the range $\phi = 0.4$–0.6, increasing the argon plasma feed gas flow rate from 0.35 slm to 0.49 slm resulted in a decrease in minimum ignition power but this had a lower bound since upon continuous increase from 0.49 slm to 0.66 slm the minimum power required for ignition is observed to increase. This trend is also observed for fuel equivalence ratios in the range 1.1–1.4. Whereas, for fuel equivalence ratios in the range, 0.7–1.0, increasing the plasma argon feed gas flow rate results in a corresponding increase in minimum ignition plasma power.

It is proposed that the trend observed for ultra-lean ($\phi = 0.4$–0.6) and rich fuel equivalence ratios ($\phi = 1.1$–1.4) is due to the turbulence effects of the plasma feed gas in the surfatron in that for fuel equivalence ratios in this range, increasing the flow rate from 0.35 slm to

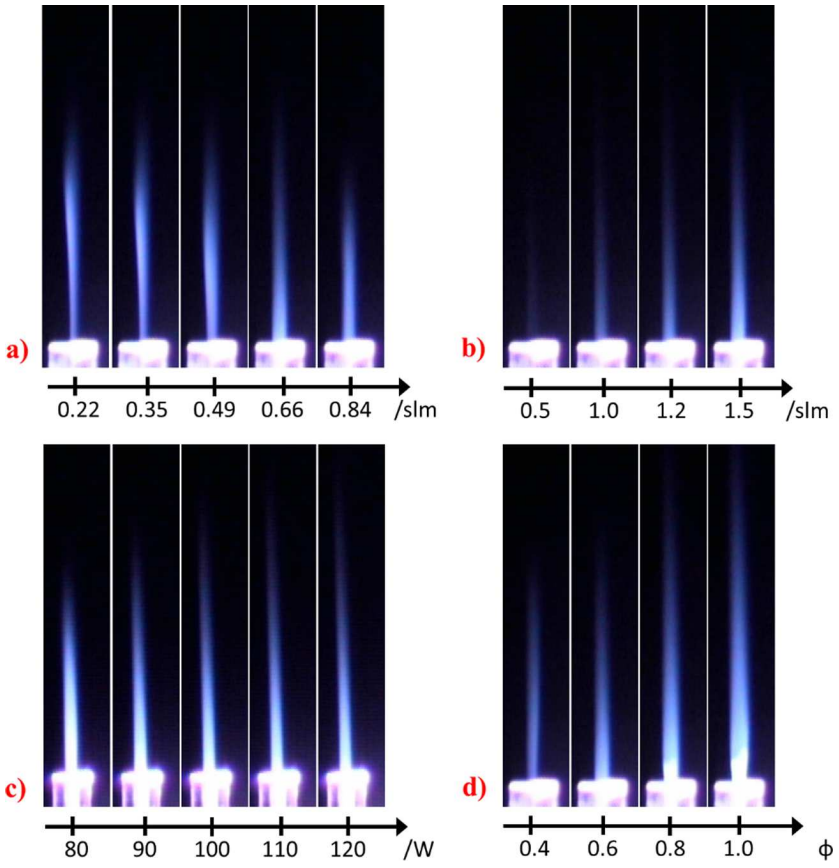

Fig. 4. (a) Variation of flame length with argon feed gas flow rate. (b) Variation in flame length with total flow rate of fuel/air mixture. (c) Variation of flame length with plasma power. (d) Variation of flame length with fuel equivalence ratio. The images above were obtained at the following fixed combustor parameters, argon feed gas flow rate of 0.66 slm, total fuel/air flow rate of 1.5 slm, plasma power of 100 W and fuel equivalence ratio of 0.6, except for when the parameter was being investigated.

0.49 slm results in an increase in radicals supplied to the plasma resulting in lower powers required for mixture ignition. However upon continuous increase of plasma feed gas flow rate, the turbulence effects experienced with increase in gas flow outweigh the enhancement due to radicals supplied therefore requiring a higher plasma power to generate the radical pool needed to ignite and hold a flame in these conditions. Whereas due to the near stoichiometric nature of fuel equivalence ratios in the range 0.7–1.1, the turbulence introduced as a result of increased plasma feed gas flow rate outweigh the benefits of radicals supplied by plasma hence for higher feed gas flow rates, a higher plasma power is needed to ignite and sustain combustion. Hence, these results suggest that ultra-lean and rich fuel equivalence ratios are more sensitive to changes in the radical pool size compared to near stoichiometric fuel equivalence ratios.

3.2 Effect on flame length

It was observed that an increase in argon plasma feed gas flow rate at a fixed plasma power of 100 W, fixed fuel equivalence ratio of 0.6 and fixed total fuel/air mixture of 1.5 slm resulted in a decrease in the flame length as shown in Figure 4a. As proposed in Section 3.1, the turbulence generated in the plasma reactor with increase plasma feed gas flow rate resulted in the observed decrease in flame height. Flame tethering was also observed with increase in the argon plasma feed gas flow rate. In a previous study [4], we investigated the role of plasma in the ignition and flameholding in ethylene/air mixtures. It was observed in that study that plasma assisted flameholding post ignition was achieved due to an increase in radical number density supplied by the plasma with increase in plasma power. In this study, increasing the plasma feed gas flow rate resulted in an increase in radical number density and a corresponding increase in flow turbulence and as a result, we observed an increased degree of flameholding due to larger radical pool supplied along with a corresponding decrease in the flame length due to the turbulence.

Increasing the total fuel/air mixture flow rate at fixed fuel equivalence ratio of 0.6, argon flow rate of 0.66 slm and plasma power of 100 W resulted in an increased in observed flame length as shown in Figure 4b. This increase in flame length is attributed to the increased amount of fuel supplied with increase in the fuel/air mixture. Combustion of the larger amount of fuel supplied with increase in fuel/air mixture flow rate resulted in an increase in the flame length observed. Hammack et al. [27] studying a non-premixed plasma assisted methane/air flame also observed an increase in flame length with increase in flow rate of the fuel/air mixture.

Figure 4c shows the variation in plasma length with plasma power at a fixed argon flow rate of 0.66 slm, fixed fuel/air mixture flow rate of 1.5 slm, and fixed fuel equivalence ratio of 0.6. It was observed that increasing the plasma power resulted in a slight increase in flame length. This slight increase in flame length is attributed to improved flameholding and fuel efficiency as discussed in Section 3.3. Increasing plasma power at constant plasma feed gas flow rate results in a larger radical pool generated and thermal energy supplied by the plasma. As a result, a higher percentage of the fuel is used up in the combustion process resulting in longer flame lengths as observed in Figure 4c. It should however be noted that the increase in flame length observed is not as significant due to the lean nature of the fuel equivalence ratio used.

Increasing the fuel equivalence ratio while keeping plasma power constant at 100 W, argon plasma feed gas flow rate at 0.66 slm and total fuel/air mixture flow rate at 1.5 slm resulted in an increase in flame length as observed in Figure 4d. An increase in the fuel equivalence ratio is similar yet different from increasing the total fuel/air mixture flow rate. The similarities lie in the fact that, increasing fuel equivalence ratio also results in more fuel available to the combustion process. The combustion of the extra fuel introduced results in a longer flame length. However they are different in that increasing the total fuel/air mixture flow rate increases both fuel and air in equal ratios while increasing the fuel equivalence ratio increases the fuel supplied while decreasing the amount of air available. As a result, for higher fuel equivalence ratio, a dual layered flame is observed as reported in our previous study [4] whereby the inner flame core which is radically rich and sustained by the plasma, ignites and stabilizes the outer flame.

3.3 Effects on fuel efficiency

Fuel efficiency as investigated in this context refers to the percentage of incoming fuel consumed in the combustor. Najm et al. [28] conducted a computational and experimental study on the use of experimental observables to measure the flame burning rate of a nitrogen diluted methane/air flame. They concluded that of all flame species investigated, HCO was found to have an excellent correlation with flame heat release rates over the range of experimental parameters investigated. Inferring from that study, the relative emission intensity of CH(A) and C_2(d) are used as experimental observables to investigate the effect of the plasma and flow parameters on the fuel efficiency of the PAC reactor. CH(A) and C_2(d) have been used previously as flame front markers [29] and in our study, due to the low fuel equivalence ratio investigated, the relative emission intensity of CH(A) and C_2(d) combined with the spatial location at which CH(A) and C_2(d) are observed along the propagation axis are used to infer the efficiency of the PAC system. Increased fuel efficiency results in a higher observed emission intensity of CH(A) and C_2(d) radicals due to a large percentage of the incoming fuel consumed in the oxidation process. Also, the spatial location at which CH(A) and C_2(d) extinction occur along the propagation axis is an indicant of the fuel efficiency of the combustion reactor operating under specific plasma and flow parameters. The relative location along the propagation axis of the occurrence of CH(A) and C_2(d) is indicant of the fuel efficiency of the PAC system, with the occurrence further downstream implying a lower fuel efficiency since fuel breakdown is still ongoing as the mechanisms of CH(A) and C_2(d) creation far outweigh the loss mechanisms.

Figure 5a shows the emission spectra obtained at different positions along the flame axis for different plasma powers at a constant fuel equivalence ratio of 0.6. The total fuel/air flow rate is fixed at 1.5 slm while the argon flow rate was fixed at 0.66 slm. It is observed that for positions $y = -12$ mm inside the combustor, the spectra from all three powers investigated feature emissions from OH($A^2\Sigma^+$–$X^2\Pi_{3/2}$)(0–0), NH($A^3\Pi$-$X^3\Sigma^-$)(0–0), CH($A^2\Delta$-$X^2\Pi$)(0–0), and C_2($d^3\Pi_g$-$a^3\Pi_u$)(0–0). With NH(A) coming from the plasma as a result of the recombination reactions of N and H due to electron impact dissociation of N_2 and H_2O in the plasma gas (R1)–(R4) [23].

$$e + H_2O \rightarrow H + OH(A, X) + e \quad (R1)$$

$$e + O_2 \rightarrow 2O + e \quad (R2)$$

$$e + N_2 \rightarrow 2N + e \quad (R3)$$

$$N + H \rightarrow NH \quad (R4)$$

$$O + H_2O \rightarrow OH + OH. \quad (R5)$$

It is proposed that OH is generated from electron impact dissociation of water molecules in the incoming gas (R1) [30,31], recombination reaction (R5), and from chain initiation and propagation reactions while CH(A) and C_2(d) are generated from chain propagation reactions [32–34].

$$C_2H + O \rightarrow CH(A) + CO \quad (R6)$$

$$C_2H + O_2 \rightarrow CH(A) + CO_2 \quad (R7)$$

$$CH_2 + C \rightarrow C_2(d) + H_2. \quad (R8)$$

At $y = -6$ mm, the emission spectra for all powers investigated feature emissions from OH($A^2\Sigma^+$–$X^2\Pi_{3/2}$)(0–0), NH($A^3\Pi$-$X^3\Sigma^-$)(0–0), CH($A^2\Delta$-$X^2\Pi$)(0–0), N_2($C^3\Pi_u$-$B^3\Pi_g$)(0–0), CN($B^2\Sigma^+$-$X^2\Sigma^+$)(0–1), and C_2($d^3\Pi_g$-$a^3\Pi_u$)(0–0) coming from the continuous chain branching reactions occurring due to continuous fuel oxidation. With N_2 coming from the energy transfer reaction when Ar($^3P_2$) from the plasma reacts with N_2 [35]

$$N_2(X^1\Sigma_g^+) + Ar(^3P_2) \rightarrow N_2(C^3\Pi_u \text{ or } B^3\Pi_g) + Ar(^1S_0). \quad (R9)$$

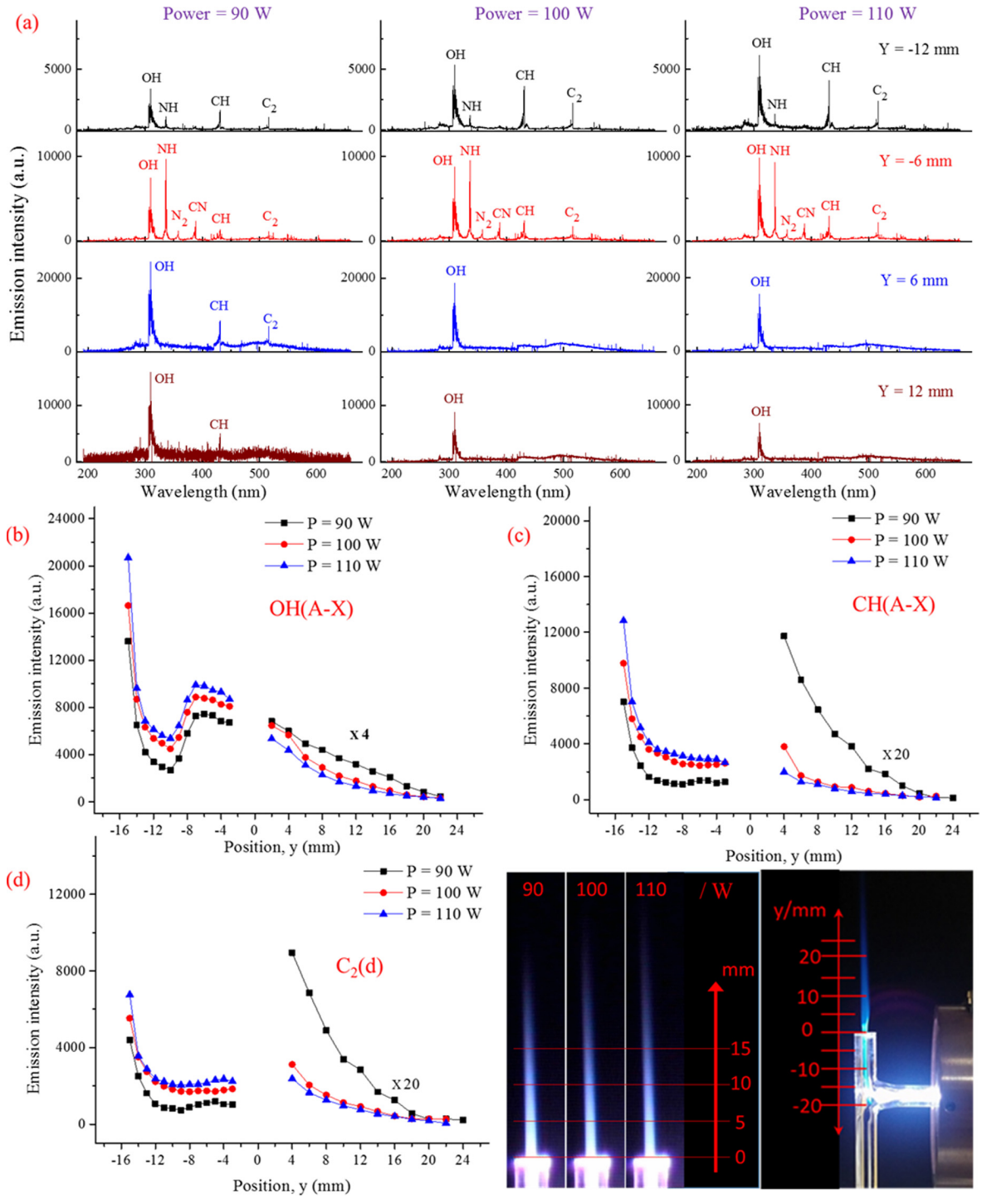

Fig. 5. (a) Emission spectra at different positions along the flame axis for different plasma powers. (b) OH($A^2\Sigma^+$–$X^2\Pi_{3/2}$)(0–0) emission intensity profile. (c) CH($A^2\Delta$-$X^2\Pi$)(0–0) emission intensity profile. (d) $C_2(d^3\Pi_g$-$a^3\Pi_u)$(0–0) emission intensity profile for plasma powers 90 W, 100 W and 110 W along the flame axis. For all data collected, the total fuel/air mixture flow rate was fixed at 1.5 slm with argon plasma gas flow rate kept constant at 0.66 slm at a fixed fuel equivalence ratio of 0.6.

At $y = 6$ mm and $y = 12$ mm, CH(A) and C_2(d) are already consumed below the detection limit of the spectrometer for powers 100 W and 110 W whereas emission spectra obtained at a plasma power of 90 W still feature emission from this species. Inferring from the presence of CH(A) and C_2(d) downstream of the flame at positions $y = 6$ mm and 12 mm for power 90 W and absence at the same spatial location for powers 100 W and 110 W, we suggest that an increase in plasma power increases the fuel efficiency of the combustor facility.

Figures 5b–5d show the emission intensity profiles for OH(A), CH(A) and C_2(d) obtained in the confined and open flame. The total fuel/air mixture flow rate, argon plasma feed gas flow rate and fuel equivalence ratio were fixed at 1.5 slm, 0.66 slm and 0.6 respectively. Inside the combustor, the integration time of the dual channel spectrometer was set to 5 s with 10 spectra obtained, averaged and recorded at a single spatial location to improve the signal to noise ratio. Outside the combustor where emission from the flame was weaker, the integration time was increased to 100 s. from the emission profiles, we observe that for OH(A-X), the emission intensity profile drops from a maximum before increasing to a secondary peak and subsequently dropping downstream along the propagation axis of the flame. This emission profile is similar to the dual peak emission feature observed in [23] where the initial drop is from the primary peak as a result of the pre ignition of the fuel/air mixture due to radicals supplied by the plasma and the lower secondary peak from the ignition of the surrounding coflow. Due to the geometry of the combustor used in this case, the primary peak is not recorded since emissions where not collected in the plasma. It is also seen that for higher plasma powers, the emission intensities for OH(A), CH(A) and C_2(d) are higher inside the combustor whereas outside the combustor, the emission intensities exhibit a reversal in trend. It is proposed that for higher powers, a larger percentage of the fuel is ignited and consumed inside the combustor resulting in more OH(A), CH(A) and C_2(d) produced as shown in Figures 5b–5d. While outside the combustor, due to a higher percentage of the fuel already consumed inside the combustor for the higher powers, the emission profile shows lower emission intensities of OH(A),CH(A) and C_2(d) for higher powers. The emission spectra in Figure 5a and emission intensity profiles in Figures 5b–5d thereby buttress that suggestion that an increase in plasma power results in improved fuel efficiency of the PAC.

Figure 6a shows the emission spectra obtained at four different locations along the flame axis for different plasma feed gas flow rates. As observed, for position $y = -12$ mm the emission spectra obtained features emissions from OH($A^2\Sigma^+$–$X^2\Pi_{3/2}$)(0–0), NH($A^3\Pi$-$X^3\Sigma^-$)(0–0), CH($A^2\Delta$-$X^2\Pi$)(0–0), and C_2($d^3\Pi_g$-$a^3\Pi_u$)(0–0). With NH(A) coming from the plasma as discussed earlier (R1)–(R4) while OH(A), CH(A) and C_2(d) are results of electron impact dissociation of water, chain branching reactions and chemiluminescence reactions (R5)–(R8). At $y = -6$ mm, the spectra obtained for plasma feed gas flow rate is mainly populated by OH(A) and NH(A) with very weak emissions coming from N_2($C^3\Pi_u$-$B^3\Pi_g$)(0–0), CN($B^2\Sigma^+$-$X^2\Sigma^+$)(0–1), CH($A^2\Delta$-$X^2\Pi$)(0–0), and C_2($d^3\Pi_g$-$a^3\Pi_u$)(0–0). Downstream of the flame, at $y = 6$ mm, the emission spectra for plasma feed gas flow rates of 0.35 slm and 0.49 slm feature emissions from OH(A) and CH(A) whereas the spectrum at the same location for a higher plasma feed gas flow rate of 0.66 slm features emission from OH(A) only. Further downstream, at $y = 12$ mm, the emission spectra for all feed gas flow rates investigated featured emissions solely from OH(A). Figures 6b–6d show the emission intensity profile for OH(A), CH and C_2(d) radicals spatially along the flame axis. The emission intensity for $y < 0$ mm inside the combustor were obtained at an integration time of 5 s while the emission intensity for $y > 0$ mm were obtained at an integration time of 100 s due to the weaker emissions from the flame. The break at $y = 0$ mm is as a result of saturation due to reflection from the edge of the combustor.

The presence of CH(A) at lower plasma feed gas flow rate and absence at a higher flow rate at $y = -6$ mm suggests that an increase in plasma feed gas flow rate improves fuel efficiency. This is inferred from the observation that, for higher plasma feed gas flow rates the emission intensities for OH(A), CH(A) and C_2(d) are higher inside the combustor ($y < 0$ mm) and lower outside ($y > 0$ mm) as compared to lower plasma feed gas flow rates where the emission intensities for OH(A), CH(A) and C_2(d) are lower inside the combustor and higher outside. Increasing the argon flow rate results in a larger radical pool supplied to the ignition zone consequently, more of the fuel is consumed inside the combustor accounting for the higher emission intensities for OH(A), CH(A) and C_2(d) observed inside the combustor for higher feed gas flow rates. The lower emission intensity profiles obtained for higher plasma feed gas flow rates outside the combustor are due to the larger percentage of the fuel consumed inside the combustor.

Figure 7a shows the emission spectra at different locations along the flame axis for different total fuel/air mixture flow rates. The plasma power, the plasma feed gas flow rate and fuel equivalence ratio were fixed at 100 W, 0.66 slm and 0.6 respectively. At position $y = -12$ mm, the emission spectra for all total fuel/air mixture flow rates were dominated by emissions from OH($A^2\Sigma^+$–$X^2\Pi_{3/2}$)(0–0), CH($A^2\Delta$-$X^2\Pi$)(0–0), and C_2($d^3\Pi_g$-$a^3\Pi_u$)(0–0), with very little emissions from NH($A^3\Pi$-$X^3\Sigma^-$)(0–0). At $y = -6$ mm the emission spectra was littered with emissions from OH($A^2\Sigma^+$–$X^2\Pi_{3/2}$)(0–0), NH($A^3\Pi$-$X^3\Sigma^-$)(0–0), N_2($C^3\Pi_u$-$B^3\Pi_g$)(0–0), CN($B^2\Sigma^+$-$X^2\Sigma^+$)(0–1), CH($A^2\Delta$-$X^2\Pi$)(0–0), and C_2($d^3\Pi_g$-$a^3\Pi_u$)(0–0). And for $y = 6$ mm and $y = 12$ mm, the emission spectra featured emissions from OH($A^2\Sigma^+$–$X^2\Pi_{3/2}$)(0–0) only. Figures 5b–5d show the emission intensity profiles for OH($A^2\Sigma^+$–$X^2\Pi_{3/2}$)(0–0), CH($A^2\Delta$-$X^2\Pi$)(0–0), and C_2($d^3\Pi_g$-$a^3\Pi_u$)(0–0). It is observed that for $y < 0$ mm, OH(A), emission intensity profile remains relatively constant with increase in total fuel/air mixture flow rate whereas CH(A) and C_2(d) show significant variation. It is observed that for lower flow rates, the CH(A) and C_2(d) emission intensity profiles quickly reach a maximum before dropping down to below detection levels with the peak emission intensity achieved dropping when the total fuel/air flow rate is increased. This trend is explained by considering the residence time of the fuel in the combustor. For lower total fuel/air mixture flow rates, the residence time of the fuel/air mixture is higher such that at this fixed plasma power, the thermal and radical contribution of the plasma is enough to oxidize a higher percentage of the fuel. Increasing the total flow rate of the fuel/air mixture results in a lower residence time and

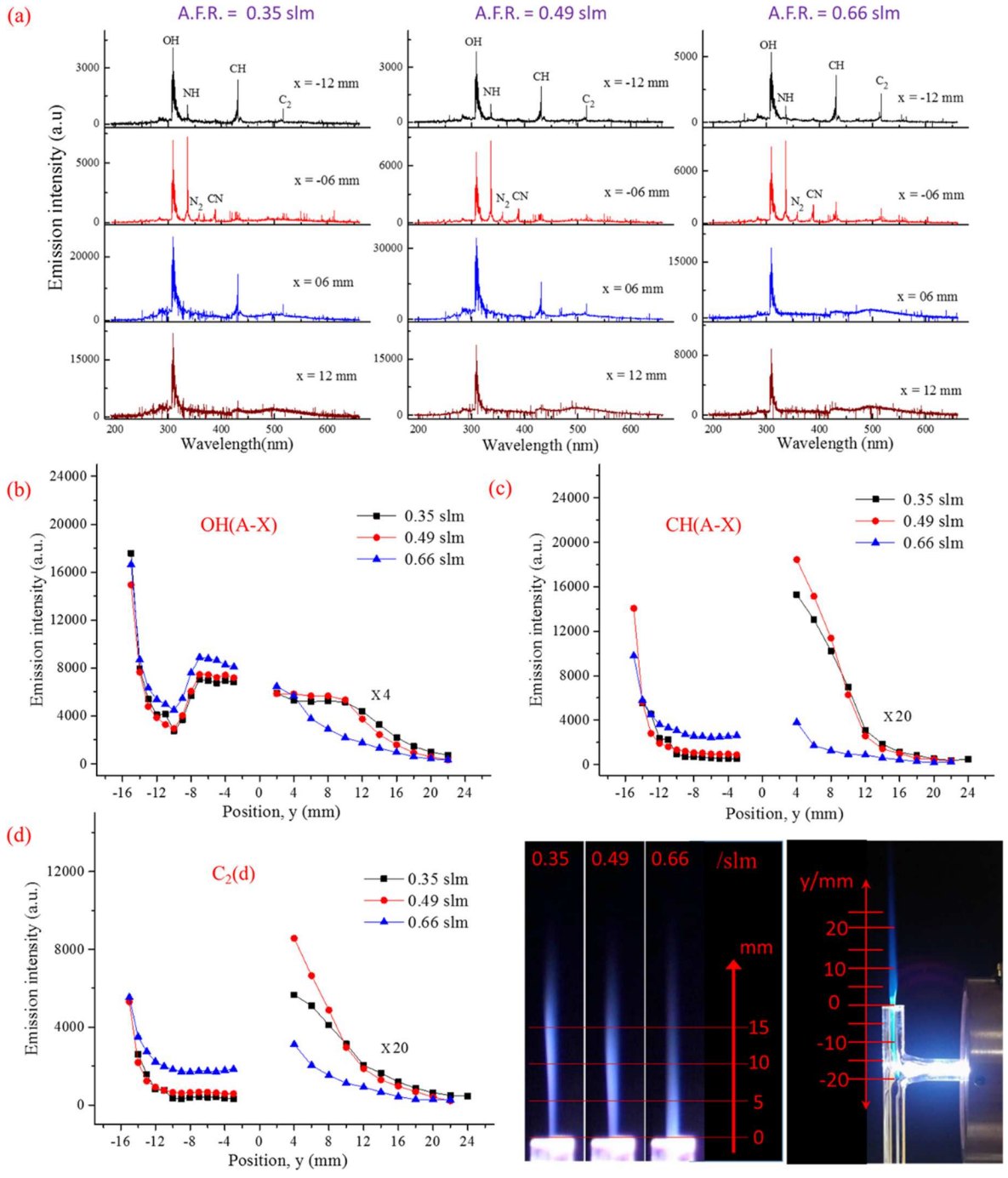

Fig. 6. (a) Emission spectra at different positions along the flame axis for different argon plasma feed gas flow rates. (b) $OH(A^2\Sigma^+–X^2\Pi_{3/2})(0–0)$ emission intensity profile. (c) $CH(A^2\Delta\text{-}X^2\Pi)(0–0)$ emission intensity profile. (d) $C_2(d^3\Pi_g\text{-}a^3\Pi_u)(0–0)$ emission intensity profile for plasma feed gas flow rates of 0.35 slm, 0.49 slm and 0.66 slm along the flame axis. For all data collected, the total fuel/air mixture flow rate was fixed at 1.5 slm with plasma power constant at 100 W at a fixed fuel equivalence ratio of 0.6.

consequently a lower percentage of the fuel oxidized in the combustor as evidenced by the decrease in peak emission intensity and the farther downstream of the flame axis at which the peak is achieved. Hence, an increase in flow rate results in a shorter residence time of the fuel inside the combustor and as a result, a lower percentage of the fuel is ignited in the combustor as seen by the reduction in the emission intensity of the peak of CH(A) and C_2(d). It is thus concluded that increasing the total fuel/air mixture flow rate at fixed plasma power results in the decrease in fuel efficiency of the combustion system.

Figure 8a shows the emission spectra obtained at different spatial locations along the flame axis for three different fuel equivalence ratios of 0.4, 0.6 and 0.8.

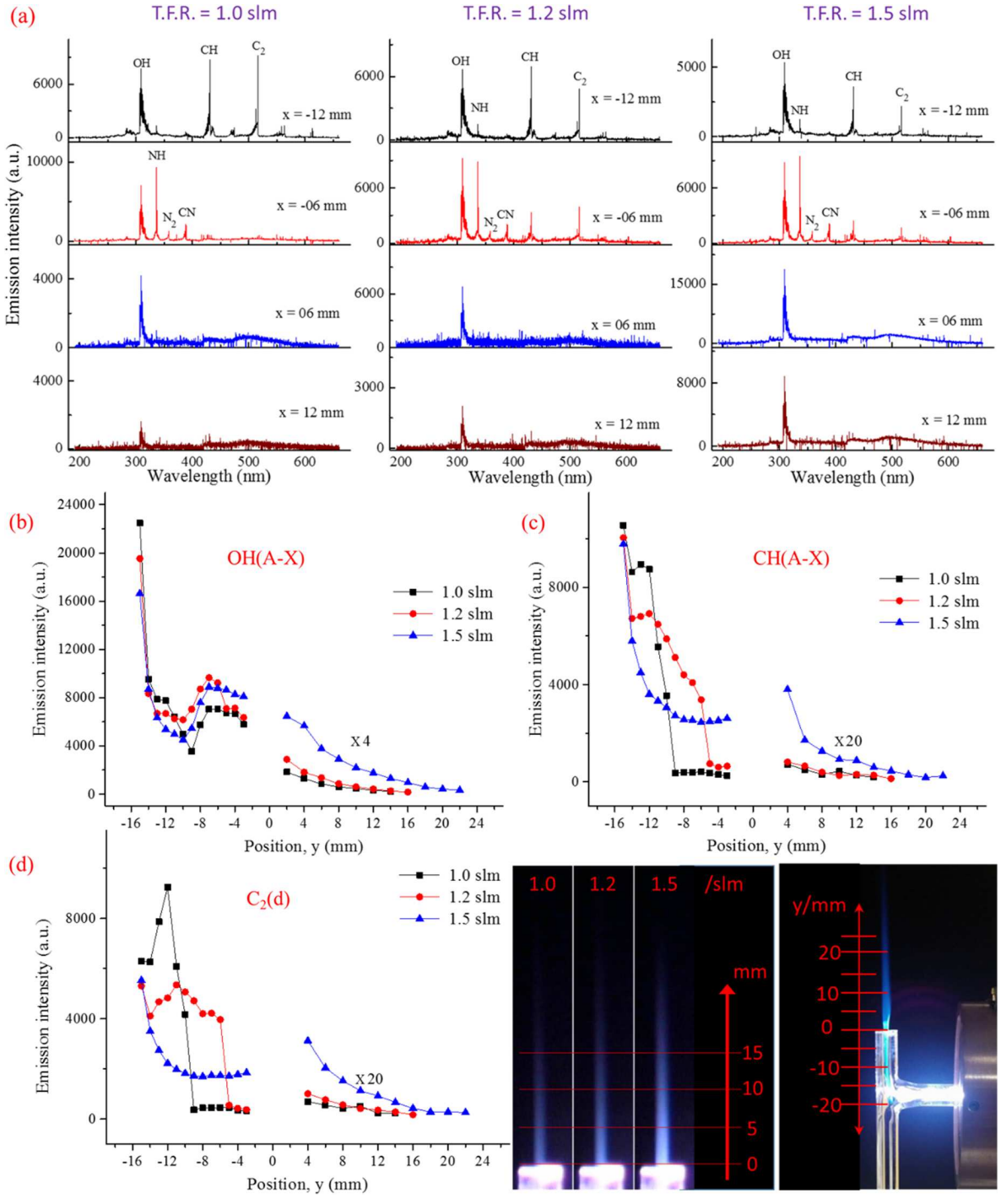

Fig. 7. (a) Emission spectra at different positions along the flame axis for different total fuel/air mixture flow rates. (b) $OH(A^2\Sigma^+–X^2\Pi_{3/2})(0–0)$ emission intensity profile. (c) $CH(A^2\Delta\text{-}X^2\Pi)(0–0)$ emission intensity profile. (d) $C_2(d^3\Pi_g\text{-}a^3\Pi_u)(0–0)$ emission intensity profile for total fuel/air mixture flow rates of 1.0 slm, 1.2 slm and 1.5 slm along the flame axis. For all data collected, the argon plasma feed gas flow rate was fixed at 0.66 slm with plasma power constant at 100 W at a fixed fuel equivalence ratio of 0.6.

The power was kept constant at 100 W along with the total fuel/air mixture flow rate and plasma feed gas flow rate at 1.5 slm and 0.66 slm respectively. At $y = -12$ mm inside the combustor, for the fuel equivalence ratio of 0.4, the emission spectra featured emissions from OH($A^2\Sigma^+$–$X^2\Pi_{3/2}$)(0–0), NH($A^3\Pi$-$X^3\Sigma^-$)(0–0), CH($A^2\Delta$-$X^2\Pi$)(0–0) but none from C_2($d^3\Pi_g$-$a^3\Pi_u$)(0–0). Upon increasing the fuel equivalence ratio to 0.6 and 0.8, the emission spectra at this spatial location featured emissions from OH($A^2\Sigma^+$–$X^2\Pi_{3/2}$)(0–0), NH($A^3\Pi$-$X^3\Sigma^-$)(0–0), CH($A^2\Delta$-$X^2\Pi$)(0–0) and an increasing presence of C_2($d^3\Pi_g$-$a^3\Pi_u$)(0–0). The same trend is observed at $y = -6$ mm where in addition to OH($A^2\Sigma^+$–$X^2\Pi_{3/2}$)(0–0), NH($A^3\Pi$-$X^3\Sigma^-$)(0–0), N_2($C^3\Pi_u$-$B^3\Pi_g$)(0–0) and CN($B^2\Sigma^+$-$X^2\Sigma^+$)(0–1) observed for lower fuel equivalence ratio of 0.4, emissions from C_2($d^3\Pi_g$-$a^3\Pi_u$)(0–0) is also observed and with the emission intensity increasing with increasing fuel equivalence ratio from 0.6 to 0.8. Downstream of the flame at $y = 6$ mm and $y = 12$ mm the only species present in the emission spectra is the OH(A) radical. Figures 5b–5d show the emission intensity profiles for OH(A), CH(A) and C_2(d) along the flame axis for the three different fuel equivalence ratios investigated. It is observed that an increase in fuel equivalence ratio results in a higher emission intensity profile for OH(A), CH(A) and C_2(d) with the increase significant for C_2(d) and CH(A). This is due to the fact that an increase in fuel equivalence ratio results in more fuel being supplied to the combustion process, as a result, a higher amount of fuel is oxidized as evidence by the increase in emission intensity of CH(A) and C_2(d). It should be noted that only lean fuel equivalence ratios are currently investigated due to the fact that, soot was deposited along the combustor walls for richer fuel equivalence ratios upon prolonged operation of the combustion system. Hence, inferring from the observation that an increase in fuel equivalence ratio resulted an increase in the emission intensities of the CH(A) and C_2(d) radicals both inside and outside the combustor, along with sooting observed upon prolonged operation for higher fuel equivalence ratios, it is concluded that, at fixed power, the fuel efficiency of the system decreases with increase in fuel equivalence ratio.

3.4 CRDS measurement of OH(X)

Part of the rotationally-resolved absorption spectra of the OH(A–X)(0–0) band near 308 nm was obtained with a spectral resolution of 0.005 nm inside the plasma plume. Assignments of the OH spectra were confirmed through comparison with the simulated spectra obtained using LIFBASE [36]. From the rotationally resolved spectra obtained, the $R_2(1)$ rotational line was selected for the ground state OH(X) number density measurements since it had no overlap with neighboring lines. After identifying and selecting the $R_2(1)$ line, a higher spectral resolution of 0.000.3 nm was used to scan ringdown spectra of the line of OH(X) in the PAC flames. Figure 9 shows the scans obtained of the OH(A–X) $R_2(1)$ line at different locations from $y = 2$ mm to $y = 20$ mm in the PAC flame of ethylene/air mixtures.

The integrated absorbance was used to calculated the OH(X) number density due to the fact that the OH $R_2(1)$ line intensity is sensitive to temperature which influences the line shape. The absolute number density in the lower rotational energy level of the $R_2(1)$ transition can be derived from the ringdown measurement using the formula,

$$\text{Integrated absorbance} = \int_\nu \frac{L}{c}\left(\frac{1}{\tau^f(\nu)} - \frac{1}{\tau_0^f}\right) d\nu = S(T)nl, \quad (1)$$

where n is the OH number density in the initial state of the $R_2(1)$ transition; $\tau^f(\nu)$ and τ_0^f are the ringdown times obtained in the PAC flames when the laser wavelength is tuned onto and off the absorption line, respectively; c is the speed of light; L and l are the ringdown cavity length and the laser beam path-length respectively. $S(T)$ is the temperature-dependent line intensity and can be calculated using equation (2) [37]

$$S(T) = 3.721963 \times 10^{-20} \frac{T(K)}{273.16} \frac{1}{8\pi c\nu^2} \left(\frac{N}{P}\right) \times \left(\frac{e^{-1.4388E''/T}}{Q_{VR}}\right) A_{\nu''J''}^{\nu'J'}(2J'+1) \times \left(1 - e^{\frac{-1.4388\nu}{T}}\right), \quad (2)$$

where T is the temperature in Kelvin, ν is the transition frequency of the OH $R_2(1)$ line of 32 415.452 cm^{-1}, N is the total number density (molecule cm^{-3}) at pressure P (atm) and temperature T, $A_{\nu''J''}^{\nu'J'}$ is the Einstein coefficient in s^{-1}, E'' is the lower state energy, i.e. 126.449 cm^{-1}, and QVR is the vibrational rotational partition function with V and J vibrational and rotational quantum numbers, respectively. The temperature dependent line intensity $S(T)$ was calculated using the temperature obtained from spectral simulations using Specair [38,39].

The measurement uncertainty of OH(X) number densities was estimated by accounting for the measurement errors in the flame temperature and the laser beam path-length. The temperature sensitivity of the line intensity of the chosen OH(A–X)(0–0) $R_2(1)$ line was approximately 5% per 100 K at 2000 K. The error in determining path-lengths was in a scale of up to 0.5 mm, which accounted for 25% of the typical path-length near 2 mm. Therefore, the overall maximum uncertainty of the measured OH(X) number densities was estimated to be ±30%.

Figure 10 shows the variation in the ground state OH(X) number density profiles with variation in each plasma and flow parameters investigated while keeping the other parameters constant. Figure 10a shows the change in the OH(X) number density profile with increase in plasma power while keeping the total fuel/air mixture flow rate constant at 1.5 slm, the argon plasma feed gas flow rate constant at 0.66 slm along with a constant fuel equivalence ratio of 0.6. It was observed that for all powers investigated, the absolute OH(X) number density decreased

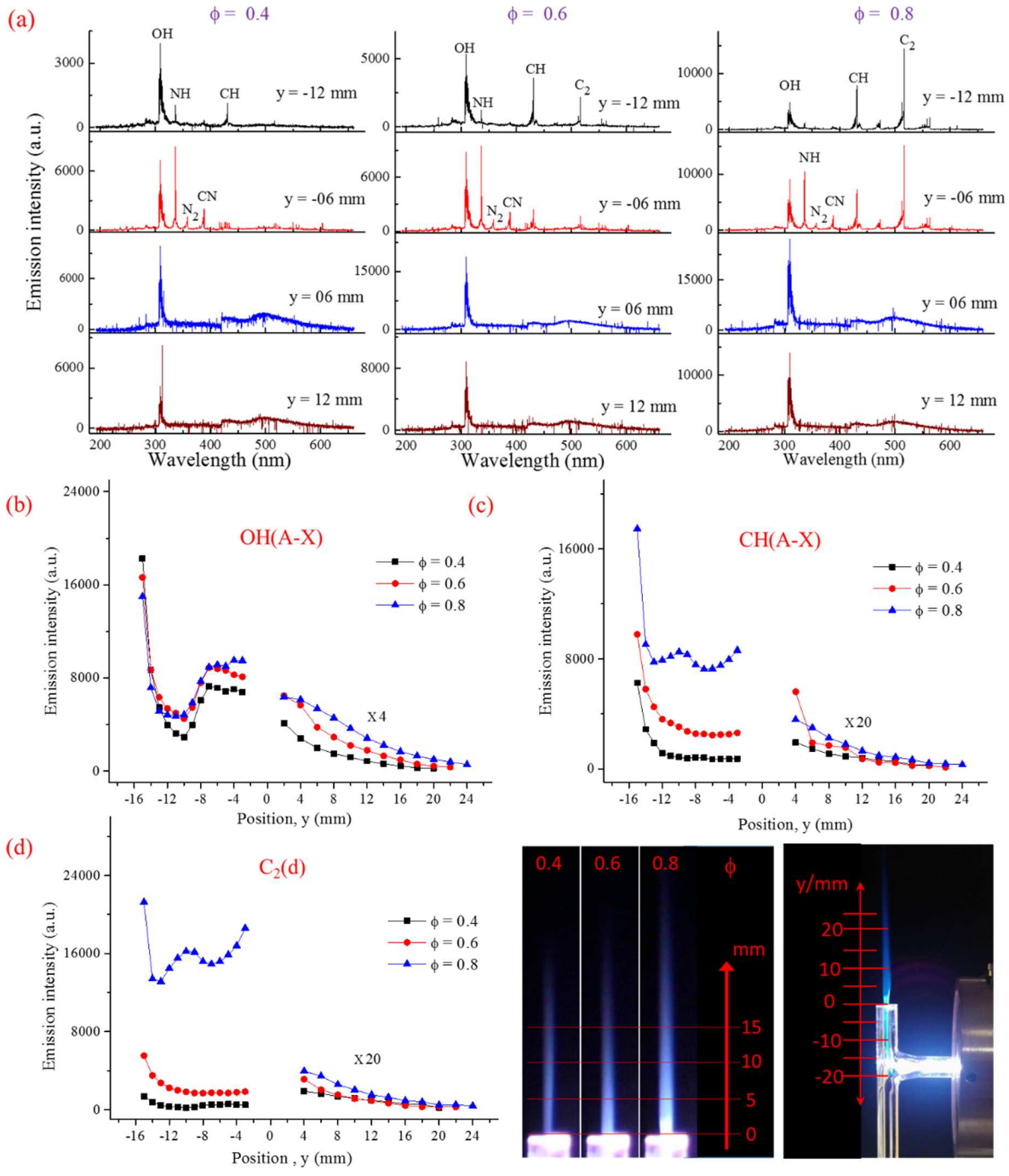

Fig. 8. (a) Emission spectra at different positions along the flame axis for different fuel equivalence ratios. (b) OH($A^2\Sigma^+$–$X^2\Pi_{3/2}$)(0–0) emission intensity profile. (c) CH($A^2\Delta$-$X^2\Pi$)(0–0) emission intensity profile. (d) C_2($d^3\Pi_g$-$a^3\Pi_u$)(0–0) emission intensity profile for fuel equivalence ratios of 0.4, 0.6 and 0.8 along the flame axis. For all data collected, the total fuel/air mixture flow rate was fixed at 1.5 slm with an argon plasma feed gas flow rate of 0.66 slm and at a plasma power constant at 100 W.

downstream spatially along the flame axis. The main OH(X) generation pathways downstream of the flame included, relaxation from excited to ground state, chain initiation and branching reactions (R10)–(R14) [40–42]. Whereas, the main OH(X) loss mechanisms were diffusion and chain termination reactions.

$$O_2 + CH_3 \rightarrow OH + CH_2O \quad \text{(R10)}$$

$$O + CH_2O \rightarrow OH + HCO \quad \text{(R11)}$$

$$CHO + O_2 \rightarrow CO + HO_2 \quad \text{(R12)}$$

$$H + HO_2 \rightarrow OH + OH \quad \text{(R13)}$$

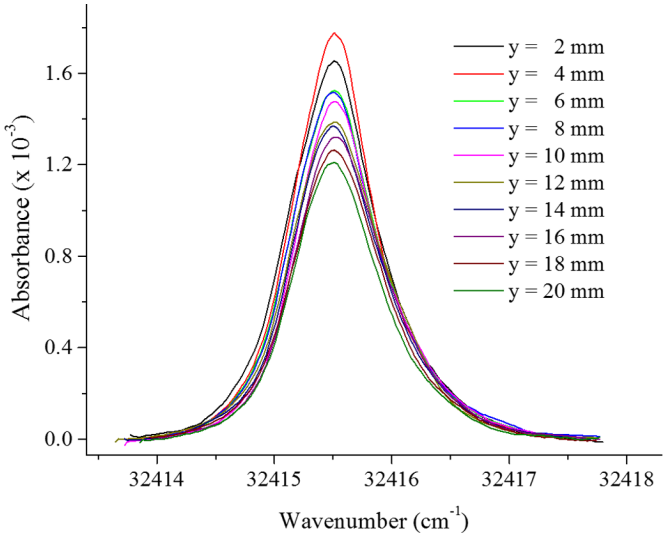

Fig. 9. The CRDS measured spectral line shapes of the $R_2(1)$ rotational line of the OH(A–X)(0–0) band at different locations from $y = 2$ mm to $y = 20$ mm in PAC flame. A ten-point adjacent-average was used. Plasma power = 100 W, $f = 0.6$, argon flow rate = 0.66 slm, and ethylene/air mixtures flow rate = 1.5 slm.

$$O + HO_2 \rightarrow OH + O_2. \quad \text{(R14)}$$

It is suggested that this decrease in OH(X) number density downstream of the flame is due to OH(X) loss through chain termination reactions and diffusion superseding OH(X) creation pathways through relaxation of OH(A) from excited state to ground state, chain initiation, and chain branching reactions.

It was also observed that an increase in plasma power did not have any effect on the OH(X) number density downstream of the flame for example at $y = 12$ mm, the OH(X) number densities were 3.8×10^{15} molecules/cm^3, 3.95×10^{15} molecules/cm^3 and 3.7×10^{15} molecules/cm^3 at plasma powers of 90 W, 100 W and 110 W respectively. Increasing the plasma power results in a larger radical pool and thermal contribution of the plasma to the ignition and combustion of the fuel/air mixture [4] and consequently, a larger percentage of the fuel is consumed. However due to the lean nature of the fuel equivalence ratio used in this study, at a plasma power of 90 W, much of the fuel is already used up in the combustion process such that increasing plasma power does not result in any significant increase of the percentage of fuel used. This hypothesis is supported by the slight increase in flame length observed in Figure 4c with increase in plasma power.

The OH(X) number densities where observed to increase to a peak value before decreasing downstream for all argon plasma feed gas flow rates investigated. With the peak achieved increasing with a decrease in plasma feed gas flow rate and the peak location occurring further downstream along the flame propagation axis with decrease in plasma feed gas flow rate as shown in Figure 10b. The fuel/air mixture flow rate was kept constant at 1.5 slm with the plasma power and fuel equivalence ratio fixed at 100 W and 0.6 respectively during this investigation. Wang and Wu [42] showed that the OH profile along the flame axis exhibited a dual peak nature where the primary peak depicted ignition onset as a result of plasma interaction while the secondary peak was due to the ignition of the surrounding coflow. The surge in OH radicals here is employed as an indicant of ignition as used in references [42,43]. Inferring from the emission data collected, the primary peak in OH(X) is achieved inside the combustor tube and hence the secondary peaks observed outside the combustor ($y > 0$ mm) in Figure 10 are due to the ignition of the surrounding coflow. Increasing the argon feed gas flow rate results in a larger radical number density supplied to the ignition zone and as a result a larger amount of fuel is consumed during the ignition onset. A larger percentage of fuel consumed during the ignition onset implies coflow heating and subsequent ignition occurs relatively earlier compared to the case when the radical pool supplied by the plasma is smaller. This accounts for why the peak at which the OH emission intensity occurs recedes toward the combustor orifice with increasing argon feed gas flow rate. The drop in the peak OH(X) number density observed is due to the fact that increasing the argon plasma feed gas flow rate results in a larger percentage of incoming fuel being consumed causing the percentage of fuel left for ignition in the surrounding coflow to be lower. As a result, the percentage of left over unignited fuel in the surrounding coflow reduces with increase in feed gas flow rate. Hence upon ignition of the surrounding coflow, the OH generated is lower for higher plasma feed gas flow rates hence the observed trend above.

Figure 10c shows the OH(X) number density profiles for total fuel/air mixture flow rates of 1.0 slm and 1.5 slm obtained along the flame propagation axis. The plasma power was fixed at 100 W and the plasma feed gas flow rate along with the fuel equivalence ratio were fixed at 0.66 slm and 0.6 respectively. The OH(X) number density decreases downstream along the flame axis for all total fuel/air mixture flow rates investigated. Higher OH(X) number density profiles where obtained for the higher fuel/air mixture flow rate. This is due to the fact that increasing the fuel/air mixture flow rate results in an increase in the fuel introduced in the system and consequently a higher concentration of OH(X) radicals is generated from the chain initiation and chain branching processes from the combustion of the fuel/air mixture.

Figure 10d shows the OH(X) number density profiles for fuel equivalence ratios of 0.4, 0.6 and 0.8 at constant plasma power, total fuel/air mixture flow rate and plasma feed gas flow rates of 100 W, 1.5 slm and 0.66 slm respectively. The OH(X) number density was observed to increase downstream of the flame with increase in fuel equivalence ratio. This is similar to the scenario in which the total fuel/air mixture flow rate was increased in that increasing the fuel/equivalence ratio results in a larger amount of fuel available to the combustion process, as a result a higher OH(X) number density is observed.

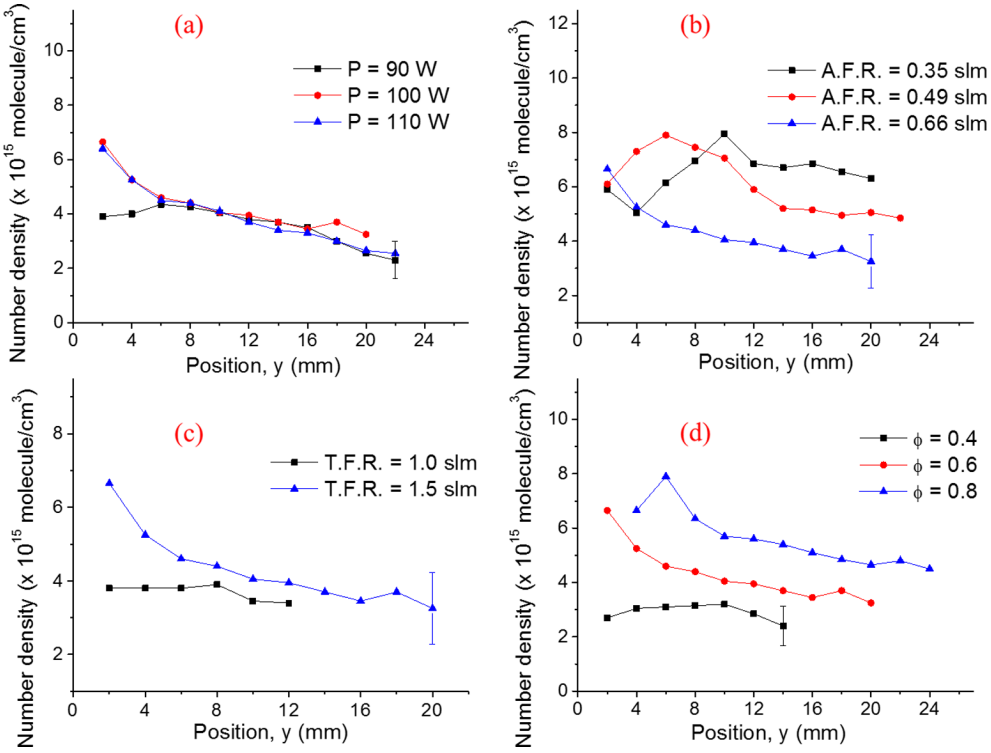

Fig. 10. Absolute OH(X) number density profiles obtained along the flame axis for: (a) Powers 90 W, 100 W, and 110 W. (b) Argon plasma feed gas flow rates of 0.35 slm, 0.49 slm, and 0.66 slm. (c) Total flow rate of 1.0 slm and 1.5 slm. (d) Fuel equivalence ratio of 0.4, 0.6, and 0.8. For all cases investigated, the combustor parameters where fixed at power of 100 W, fuel equivalence ratio of 0.6 total flow rate of 1.5 slm and plasma feed gas flow rate of 0.66 slm unless the parameter was under investigation.

4 Conclusion

A parametric study was performed to investigate how the plasma and fuel/air mixture parameters influence the enhancement effects observed in PAC. The parameters investigated included the plasma power, the plasma feed gas flow rate, the total fuel/air mixture flow rate and the fuel equivalence ratio. The enhancement effects of the plasma on the combustion process monitored during the parametric investigation were the minimum ignition power, flame length, and the fuel efficiency of the combustion process. Visual imaging, OES and CRDS were employed in this study. The effects of each parameter investigated based on the enhancement criteria chosen are presented. It was observed that increasing the argon plasma feed gas flow rate resulted in improved flame stability due to a larger radical pool generated and a corresponding decrease in flame length due to increase in turbulence in the combustor. Data obtained from OES showed a decrease in the emission intensity of CH(A) and C_2(d) downstream of the flame with increase in plasma feed gas flow rate indicant of improved fuel efficiency. Increasing the argon plasma flow rate resulted in an increase in radicals supplied to the ignition zone and a corresponding increase in turbulence in the combustor due to the higher flow rates. The minimum ignition plasma power for near stoichiometric fuel equivalence ratios was more influenced by the turbulent effects since a higher plasma power was required to ignite this mixtures with increase in plasma feed gas flow rate whereas for ultra-lean and rich fuel equivalence ratios the enhancement effects due to the larger radical pool supplied outweighed the turbulence effects generated in the flow. Increasing the plasma power resulted in a slight increase in the plasma flame length due to the low fuel equivalence ratio investigated along with an improvement in the fuel efficiency inferred from the decrease in the emission intensities of CH(A) and C_2(d) downstream of the flame. Increasing the total fuel/air mixture flow rate or fuel equivalence ratio resulted in longer flame lengths observed and corresponding decreases in fuel efficiencies of the PAC system. Outside the combustor the OH(X) absolute number density was on the order of 10^{15} molecules/cm^3 and was observed to decrease downstream of the flame for all parameters investigated. We have thus employed the minimum ignition plasma power, the flame length and the fuel efficiency of the combustion facility as the criteria for combustion enhancement, to investigate and characterize how four different experimental variables – the argon plasma feed gas flow rate, plasma power, fuel equivalence ratio and total fuel/air mixture flow rate – independently influence the PAC process in a bid to shed more light on this phenomenon.

This work was supported by the National Science Foundation through the grant CBET-1066486.

Author contribution statement

Che A. Fuh and Wei Wu collected and analyzed the experimental data. Che A. Fuh wrote up the manuscript. Chuji Wang formulated the research idea and helped with the data interpretation and the manuscript write up.

References

1. J.B.J. Michael, T.L.T. Chang, R.R.B. Miles, Combust. Flame **160**, 796 (2013)
2. W. Wu, C.A. Fuh, C. Wang, Combust. Sci. Technol. **187**, 999 (2015)
3. K.W. Hemawan, C.L. Romel, S. Zuo, I.S. Wichman, T.A. Grotjohn, J. Asmussen, Appl. Phys. Lett. **89**, 141501 (2006)
4. C.A. Fuh, W. Wu, C. Wang, J. Phys. D: Appl. Phys. **49**, 285202 (2016)
5. W. Kim, H. Do, M.G. Mungal, M.A. Cappelli, in *44th AIAA Aerospace Sciences Meeting and Exhibit, Reno* (2006)
6. M.G. De Giorgi, A. Sciolti, S. Campilongo, E. Pescini, A. Ficarella, S. Lovascio, G. Dilecce, IEEE Sens. J. **16**, 3896 (2016)
7. J.P. Moeck, D.A. Lacoste, D. Durox, T.F. Guiberti, T. Schuller, C.O. Laux, IEEE Trans. Plasma Sci. **42**, 2412 (2014)
8. Z. Yin, I. Adamovich, in *49th AIAA Aerosp. Sci. Meet. Incl. New Horizons Forum Aerosp. Expo., Orlando* (2011)
9. J.B. Liu, J. Sinibaldi, C. Brophy, A. Kuthi, C. Jiang, P. Ronney, M.A. Gundersen, IEEE Trans. Plasma Sci. **33**, 844 (2005)
10. S. Nagaraja, W. Sun, V. Yang, Proc. Combust. Inst. **35**, 3497 (2014)
11. R.A. Varella, J.C. Sagás, C.A. Martins, Fuel **184**, 269 (2016)
12. T. Yamamoto, T. Tsuboi, Y. Iwama, R. Tanaka, Energy Fuels **30**, 3495 (2016)
13. J. Hwang, C. Bae, J. Park, W. Choe, J. Cha, Combust. Flame **167**, 86 (2016)
14. A. Bao, Y.G. Utkin, S. Keshav, G. Lou, I.V. Adamovich, IEEE Trans. Plasma Sci. **35**, 1628 (2007)
15. N. Chintala, A. Bao, G. Lou, I.V. Adamovich, Combust. Flame **144**, 744 (2006)
16. N. Ezumi, K. Akahane, K. Sawada, Y. Tanaka, M. Tanaka, T. Uda, K. Nishimura, Plasma Fusion Res. **7**, 2401075 (2012)
17. W. Wu, C.A. Fuh, C. Wang, IEEE Trans. Plasma Sci. **43**, 3986 (2015)
18. C. Fuh, W. Wu, C. Wang, in *45th AIAA Plasmadynamics and Lasers Conference, Atlanta* (2014)
19. W. Sun, Y. Ju, J. Plasma Fusion Res. **89**, 208 (2013)
20. A. Starikovskiy, in *31st ICPIG, Grenada* (2013)
21. A. Starikovskiy, N. Aleksandrov, Prog. Energy Combust. Sci. **39**, 61 (2013)
22. C. Wang, J. Anal. At. Spectrom. **22**, 1347 (2007)
23. C. Wang, W. Wu, J. Phys. D: Appl. Phys. **46**, 464008 (2013)
24. N. Srivastava, C. Wang, IEEE Trans. Plasma Sci. **39**, 918 (2011)
25. C.A. Fuh, S.M. Clark, W. Wu, C. Wang, J. Appl. Phys. **120**, 16330 (2016)
26. D.J. Jin, H.S. Uhm, G. Cho, Phys. Plasmas **20**, 83513 (2013)
27. S. Hammack, T. Lee, C. Carter, IEEE Trans. Plasma Sci. **40**, 3139 (2012)
28. H.N. Najm, P.H. Paul, C.J. Mueller, P.S. Wyckoff, Combust. Flame **113**, 312 (1998)
29. Y. Ikeda, H. Nishihara, T. Nakajima, Trans. J. Engines **724** (2001)
30. P. Bruggeman, D.C. Schram, Plasma Sources Sci. Technol. **19**, 45025 (2010)
31. N. Srivastava, C. Wang, J. Appl. Phys. **110**, 53304 (2011)
32. I. Glassman, R.A. Yetter, *Combustion*, 4th edn. (Academic Press, 2008)
33. J. Grebe, K.H. Homann, Ber. Bunsenges. Phys. Chem. **86**, 587 (1982)
34. G.P. Smith, C. Park, J. Schneiderman, J. Luque, Combust. Flame **141**, 66 (2005)
35. J.L. Jauberteau, I. Jauberteau, M.J. Cinelli, J. Aubreton, New J. Phys. **4**, 39 (2002)
36. J. Luque, D.R. Crosley, LIFBASE: Database and spectral simulation (version 1.5), SRI International Report MP 99-009, 1999
37. A. Goldman, J.R. Gillis, J. Quant. Spectrosc. Radiat. Transf. **25**, 111 (1981)
38. C.O. Laux, T.G. Spence, C.H. Kruger, R.N. Zare, Plasma Sources Sci. Technol. **12**, 125 (2003)
39. G.D. Stancu, F. Kaddouri, D.A. Lacoste, C.O. Laux, J. Phys. D: Appl. Phys. **43**, 124002 (2010)
40. W. Sun, S.H. Won, T. Ombrello, C. Carter, Y. Ju, Proc. Combust. Inst. **34**, 847 (2013)
41. K.V. Artem'ev, S.Y. Kazantsev, N.G. Kononov, I.A. Kossyi, N.I. Malykh, N.A. Popov, N.M. Tarasova, E.A. Filimonova, K.N. Firsov, J. Phys. D: Appl. Phys. **46**, 55201 (2013)
42. C. Wang, W. Wu, Combust. Flame **161**, 2073 (2014)
43. S. Nagaraja, V. Yang, Z. Yin, I. Adamovich, Combust. Flame **161**, 1026 (2014)